# Functional Precision Medicine Using MicroOrganoSpheres for Treatment Response Prediction in Advanced Colorectal Cancer

Roán Gobits, MSc[1]; Nikolai Schleußner, PhD[2,3]; Gavin R. Oliver, PhD[4]; Michael Rutenberg Schoenberg, PhD[4]; António Miguel de Jesus Domingues, PhD[1]; Pavan Ramkumar, PhD[4]; Sylvia W.F. Suen, MSc[1]; Mandy P.M. Koomen, MSc[1]; Francesca Paolucci, MSc[1]; Kilian Martens, BSc[1]; Aitana Guiseris Martinez, MSc[2,5,6]; Julia Volk, MSc[2,5]; Carolin Artmann, MSc[2,5]; Manuel Mastel, MSc[2,5,6]; Kyanna S. Ouyang, MSc[7,8,9]; Matthias Kloor, PhD[10]; Eric Daniel Bankaitis, PhD[4]; Hayden Eric Stoub, MSc[4]; Jens Puschhof, PhD[7,8,9]; Kevin Brown, PhD[4]; Sebastian Pretzer, BA[4]; Daniel A. Nelson, PhD[4]; Eric Struminger, BSc[4]; Amelia Zessin, MSc[4]; Amanda Brown, BSc[4]; Corey Evans, MSc[4]; Daniel Yetsko, MSc[4]; Mackenzie Harrington, BSc[4]; Gabriel Salg, MSc[3]; Martin Schneider, PhD[3]; Thomas Schmidt, PhD[3]; Elena Helman, PhD[4]; Dennis Plenker, PhD[4]; Carlton Barnett, PhD[4]; Ryan T. Jones, PhD[4]; Bruno Köhler, PhD[11,12]; Else Driehuis, PhD[1]; and Rene Jackstadt, PhD[2,5,13]

DOI https://doi.org/10.1200/PO-25-00501

## ABSTRACT

**PURPOSE** Neoadjuvant chemotherapy is a key component of curative treatment in advanced colorectal cancer (CRC). However, 30%-40% of patients show progression on treatment, underscoring the need for predictive tools to guide up-front treatment selection. Scalable and reproducible methods for patient stratification remain limited. MicroOrganoSpheres (MOS) are droplet-encapsulated 3D tumor models that allow for high-throughput functional drug testing. Here, we evaluate the potential of tumor-derived MOS to predict response to chemotherapy in patients with CRC.

**METHODS** MOS droplets were generated from 37 primary and/or metastatic tumor samples collected from 21 patients. MOS response to chemotherapy was quantified using AI-based imaging analysis and compared with clinical response (RECIST/disease-free survival [DFS]) and lesion-specific outcomes (pathologic response/percent tumor volume change).

**RESULTS** MOS chemoprediction assay showed high reproducibility (coefficients of variation ≤ 2.5%). MOS drug sensitivity recapitulated patient response with 83% accuracy in the full sample cohort and 100% accuracy when derived from primary tumors. Patients with sensitive MOS showed longer DFS. Individual MOS analysis revealed preservation of intratumor heterogeneity in vitro and enabled identification of drug-resistant clones.

**CONCLUSION** MOS technology offers a scalable and robust functional precision medicine platform with potential to guide clinical decision making in CRC. The platform accurately predicts patient response to chemotherapy and provides insights into intrapatient and intratumor heterogeneity.

ACCOMPANYING CONTENT

Data Sharing Statement

Data Supplement

Accepted December 10, 2025
Published January 15, 2026

JCO Precis Oncol 10:e2500501




## INTRODUCTION

Colorectal cancer (CRC) is the third most common cancer type and second-leading cause of cancer-related death.[1,2] Prognosis for advanced-stage disease remains poor, with only 14% 5-year overall survival for metastatic cases.[3] Curative treatment may combine surgery with doublet or triplet chemotherapy for selected cases. Neoadjuvant therapy may improve surgical outcomes, reduce total chemotherapy administered, and lower the likelihood for local recurrence.[4,5] However, its role relative to adjuvant therapy remains debated.[6,7] Standard chemotherapy regimens (infusional fluorouracil (5-FU), leucovorin, and oxaliplatin [FOLFOX]/5-FU, leucovorin, and irinotecan [FOLFIRI]/5-FU, leucovorin, oxaliplatin, and irinotecan [FOLFOXIRI]) achieve an initial response rate of 60%, yet disease progression within 2 years is common.[8,9] To date, no validated biomarkers can reliably guide chemotherapy selection. Therefore, treatment decisions remain based on clinicopathologic features and treatment history.[10-13] This underscores the need for functional assays that can predict individual patient response and enable personalized treatment decisions.

## CONTEXT

**Key Objective**

We evaluated the application of MicroOrganoSpheres (MOS) in an ex vivo functional precision medicine platform to predict lesion- and patient-level clinical response to neoadjuvant combination chemotherapy in patients with advanced-stage colorectal cancer (CRC).

**Knowledge Generated**

MOS recapitulated clinical drug response with 83% accuracy. In addition, image-based in vitro drug response assessment offered insights into intratumoral response heterogeneity and enabled the identification of drug-resistant clones.

**Relevance**

MOS-based testing may inform treatment decisions for patients with advanced-stage CRC, where relapse rates remain high. Moreover, the standardized and automated workflow could expedite the application of functional precision medicine screening into clinical practice.



Patient-derived tumor organoids (PDTOs) are a valuable tool to model treatment response.[14-16] Multiple studies have shown that PDTOs can predict clinical responses to chemotherapeutic agents.[15-18] However, adoption into clinical practice remains hampered by the time required to obtain sufficient biomass, labor- and cost-intensive workflows, and dependence on skilled personnel, hindering standardization across clinical centers.[15,19,20] As such, automated assays are critical to enable integration of PDTO assays into routine diagnostics.

Here, we demonstrate the clinical utility of a MicroOrganoSphere (MOS)-based functional precision oncology platform,[21] which enables standardized and automated patient-specific cancer model generation and drug screening using microfluidic droplet encapsulation of dissociated tumor cells or PDTOs. Building on proof-of-concept data,[21,22] here, we have applied MOS-based screening to a larger retrospective clinically annotated cohort of patients with CRC to evaluate its potential to inform clinical decision making. In addition, we used image-based single-MOS analysis to study intratumoral heterogeneity in chemotherapy response in vitro.

## METHODS

Detailed methods are provided in the Data Supplement.

### Patients and Specimens

The study cohort comprised 33 patients with stage III and IV CRC treated with standard-of-care neoadjuvant combination chemotherapy, followed by curative-intent surgery. The study received approval by the local medical ethics committee (S-136/2021 and S-708/2019), and all patients provided written informed consent for data and tissue collection and analysis. A total of 66 primary and/or metastatic resected tumor specimens were collected. Detailed patient and sample characteristics are provided in the Data Supplement (Tables S1 and S2).

### Tumor Tissue Processing and Ex Vivo Drug Sensitivity Testing

On the day of surgery, tumor samples were dissociated and cryopreserved. Dissociated cells were thawed and expanded to PDTOs in tumor-selective medium. PDTOs were expanded to sufficient biomass and subsequently dissociated into single cells, resuspended in Matrigel, and packed into MOS droplets using the MOS generator V4.2 (20 cells/MOS). After a 2-day recovery, MOS were dispensed into 384-well plates (40 MOS/well), together with a fluorophore-conjugated EpCAM antibody using an automated liquid handler. 5-FU, oxaliplatin, and SN-38 were added to the plate in a nine-point dose gradient as single agents and in clinically relevant combinations. Brightfield and fluorescence images were acquired using a high-throughput confocal microscope on days 0, 3, and 4. The total duration of the assay from MOS generation to the end point was 7 days.

### MOS Drug Sensitivity Analysis

Individual MOS droplets were segmented from brightfield images of the assay plates using a custom deep neural network model. Within the masks generated through segmentation, EpCAM fluorescence integrals were calculated per MOS at each time point and subsequently normalized to initial assay intensities to correct for differences in biomass at the assay starting time point. In vitro drug sensitivity was determined by computing the viability for each drug-treated condition relative to the sample-specific vehicle and kill

controls. $pIC_{50}$ values were calculated from fitted dose-response curves for each sample and treatment. Subsequent ranking of all models from sensitive to resistant resulted in a MOS drug response score as a measurement of relative model sensitivity.

### Correlation With Patient Response and Statistical Testing

Binary tumor-level clinical response was determined by radiologic response for metastatic tumors (≥20% growth = Progression, consistent with RECIST thresholds[23]) and by pathologic regression based on Dworak score (tumor regression grade [TRG]0 = Progression; TRG1-4 = Response[24]) for primary tumors. Clinical response was correlated with individual MOS drug response scores. Wilcoxon rank-sum tests were used to compare response groups, and *P* values were adjusted for multiple comparisons using the Benjamini-Hochberg method. A patient-level permutation analysis was implemented to account for nonindependence of multiple lesions contributed by the same patient under the null hypothesis of no association.

Receiver operating characteristic (ROC) analysis was performed to evaluate the ability of $pIC_{50}$ values to discriminate clinical response. AUC was calculated with 95% CI estimated by bootstrap resampling under a binormal model.

MOS drug response scores were correlated with patient-level disease-free survival (DFS) from the date of surgery using Kaplan-Meier visualizations. Groups (≤50 and >50th percentile) were compared using the Mantel-Cox log-rank test. *P* values were adjusted for multiple comparisons using the Benjamini-Hochberg method.

## RESULTS

### Validation of the MOS Functional Precision Oncology Screening Platform

Here, we validated the clinical utility of the MOS screening platform[21,22] (Fig 1A). The automated, high-throughput screening pipeline consisted of a MOSgen microfluidic device (Fig 1B, Data Supplement, Fig S1 and Video S1) integrated into a robotic laboratory workflow. Readout of drug sensitivity was quantified using an AI-based imaging analysis pipeline (Fig 1C, Data Supplement, Video S2) comprising (1) a machine learning–based droplet segmentation model that segments each MOS droplet from brightfield images, (2) a signal extraction method that quantifies fluorescent markers for each segmented MOS droplet, and (3) a statistical analysis method that normalizes the extracted signal to generate dose-response curves. To assess assay reproducibility, in vitro chemotherapy sensitivity of an established CRC PDTO MOS model was determined 35 times over the course of 22 weeks, with screening performed by six independent operators. The coefficients of variation (CV) of the $pIC_{50}$ values for all five single-agent and drug combinations tested (Fig 1D) were ≤2.5% (range, 1.7%-2.5%), which is notably lower than the established acceptance threshold of <10% for complex cellular assays.[25,26] Based on these results, we proceeded with testing the drug sensitivity in a clinically annotated retrospective cohort of patient-derived tumor samples.

### Establishing MOS Models From Tumor Samples Derived From Patients Treated With Neoadjuvant Chemotherapy

#### *Clinical Sample Processing and MOS Generation*

Post-treatment resections of patients with CRC who received standard-of-care neoadjuvant chemotherapy were dissociated and cryopreserved as single cells on the day of surgery. The median sample viability was 65.5% postdissociation and 58.7% post-thawing (Data Supplement, Fig S2A), with a median cryopreservation-induced change of −4.7% (Data Supplement, Fig S2B). PDTOs were established (using previously described methods[27]) from thawed tumor material. Thirty-nine PDTOs were processed into MOS droplets and subsequently drug screened (MOS generation success rate: 100%). Based on post-readout screening data QC (Detailed Methods), two were excluded from downstream analysis (assay success rate: 95%), leaving 37 models (from 21 patients) to be included in the correlation analysis (Data Supplement, Fig S2C).

#### *Clinical Characteristics of Included MOS Models*

Of 37 included MOS models, 25 were derived from liver metastases, two from lymph node metastases, and 10 from primary tumors (Fig 2A). Most lesions were obtained from patients diagnosed with UICC Stage IV CRC, with the anatomic site of the primary tumor being colon for 19 of 37 (51%) samples and rectum for the remaining 18. Twenty-five of 37 (68%) samples were derived from patients treated with FOLFOX, 6 of 37 (16%) were derived from patients with FOLFIRI, and 6 of 37 (16%) were derived from patients with FOLFOXIRI. For 10 of 21 (48%) patients, more than one lesion was included (Fig 2B). Detailed patient characteristics are shown in the Data Supplement (Tables S1 and S2).

#### *PDTO Tumor Status Confirmation by Histology and Whole-Exome Sequencing*

We confirmed the retainment of histopathologic features of the original CRC tumor tissue in the generated PDTOs using immunohistochemistry (Fig 2C, Data Supplement, Fig S2D). To genetically confirm the tumor status of the generated models, whole-exome sequencing was performed on PDTO-derived DNA where available (n = 34). For all analyzed models, tumor status was confirmed by detection of known CRC driver mutations[28] (Fig 2D, Data Supplement, Table S3). Frequency of detected mutations in PDTOs was comparable with those reported for metastatic CRC samples.[29] *APC*, *TP53*, and *KRAS* were the most prevalently mutated genes in the cohort (94%, 62%, and 47% of samples, respectively). We

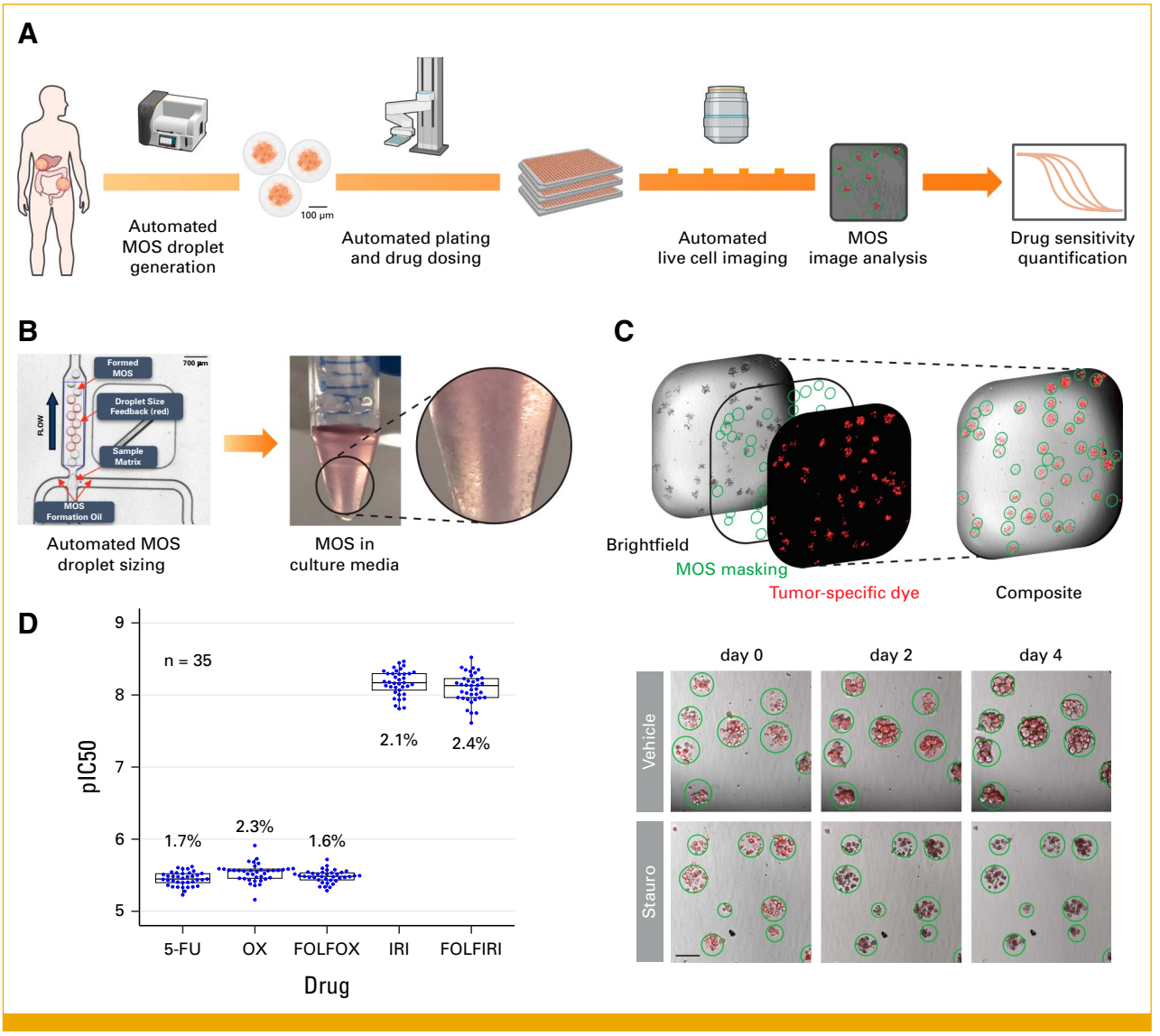


**FIG 1.** MOS functional precision oncology screening platform. (A) Schematic representation of the MOS precision medicine screening platform used in this study. The visual illustrates the workflow from the patient sample (left) to in vitro drug sensitivity quantification (right). (B) Highlights of novel features of the MOSgen device used in this study, integrated since earlier publications.[21,22] Image-based MOS droplet size adjustment (left), MOS droplet output in culture medium (right). (C) Top: different imaging readouts acquired/generated during MOS drug sensitivity screening. From left to right: brightfield image, MOS-droplet detection and segmentation algorithm, EpCAM-based fluorescence signal used for tumor cell viability quantification, three channels composited. Bottom: examples of MOS image readouts on the day of dosing (left), at 60 hours (middle), and at the end point of 96 hours (right) with negative vehicle control (DMSO; top) and positive kill control (staurosporine, STAURO; bottom). MOS detection output is indicated in green circles, and EpCAM fluorescence signal in red. Scale bar = 200 µm. (D) $pIC_{50}$ values (*y*-axis) obtained by screening an identical (control) MOS model for different chemotherapy single agents and combinations (*x*-axis) to assess assay precision. Shown % indicates CV. Y-axis $pIC_{50}$ values are in molar. 5-FU, 5-fluorouracil; CV, coefficients of variation; DMSO, dimethyl sulfoxide; FOLFIRI, fluorouracil, leucovorin, and irinotecan; FOLFOX, infusional fluorouracil, leucovorin, and oxaliplatin; MOS, MicroOrganoSphere.

confirmed that the PDTO with the highest mutational burden (S8), which came from a patient with clinically diagnosed DNA mismatch repair deficiency, indeed harbored a pathogenic p.Arg621* *MSH2* mutation. Finally, sequencing of lesions obtained from different anatomic sites within the same patient revealed shared driver mutations, alongside lesion-specific mutations in metastases, indicating continuous genetic evolution of metastases in vivo (Data Supplement, Table S3).

## In Vitro MOS Response Recapitulates Patient Response to Chemotherapy

### *Determining MOS Droplet Drug Sensitivity*

All 37 samples were evaluated for sensitivity to combination chemotherapies, including the therapy received by patients during their treatment course. In vitro MOS model sensitivity was determined by calculating the relative viability for each

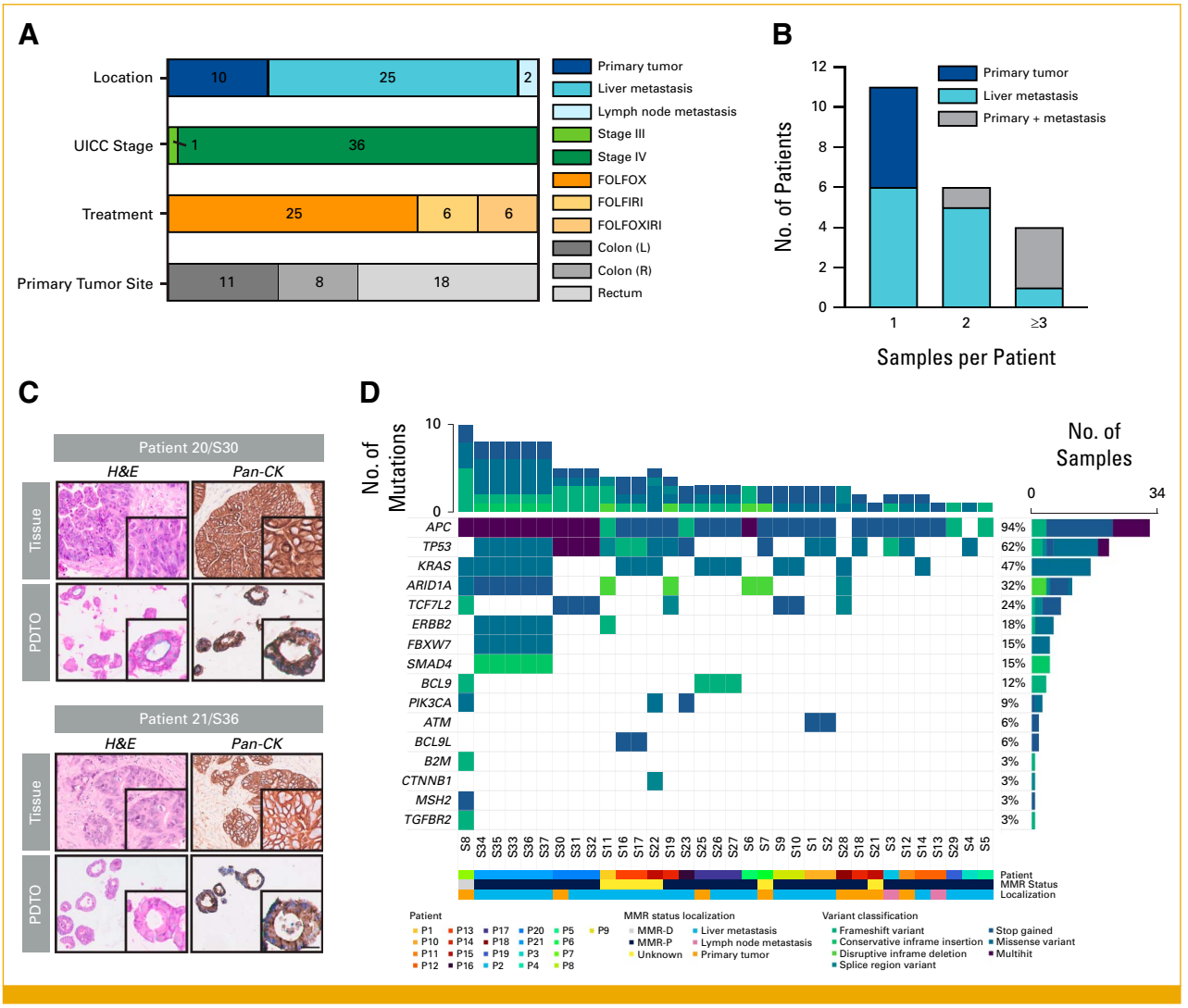


**FIG 2.** Establishment of a MOS model cohort from tumor samples of patients with colorectal cancer and characterization. (A) Clinical characteristics of 37 samples derived from 21 patients. From top to bottom: Tumor sampling location (primary tumor, liver metastasis, lymph node metastasis). Patient disease stage at the time of surgery, following UICC criteria (stage III: locoregionally advanced disease, stage IV: metastatic disease). Neoadjuvant chemotherapy regimen given to the patient (FOLFOX, FOLFIRI, FOLFOXIRI). Anatomic location of primary tumor (Colon [L] = left descending colon, Colon [R]: right ascending colon). (B) Histogram indicating the number and sampling location of specimens obtained for each included patient: Number of patients (*y*-axis), number of tumor samples per patient (*x*-axis). Colors indicate the anatomic location of the sample(s) included for each patient. (C) H&E staining and Pan-CK of primary tumor tissue and corresponding generated PDTOs from two patients (P20/S30 and P21/S36). Scale bar = 25 μm. (D) Oncoplot of mutations detected by WES of 34 PDTO models. Top panel, the total number of mutations found in the PDTO for the genes shown. Right panel, the percentage of samples in which a particular gene was mutated. FOLFIRI, infusional fluorouracil, leucovorin, and irinotecan; FOLFOX, infusional fluorouracil, leucovorin, and oxaliplatin; FOLFOXIRI, infusional fluorouracil, leucovorin, oxaliplatin, and irinotecan; H&E, hematoxylin & eosin; MMR-D, mismatch repair–deficient; MMR-P, mismatch repair–proficient; MOS, MicroOrganoSphere; Pan-CK, pan-cytokeratin; PDTOs, patient-derived tumor organoids; UICC, union for international cancer control; WES, whole-exome sequencing.

drug-treated condition using EpCAM fluorescence intensity (Methods) and fitting dose-response curves (Fig 3A). Response was quantified by ranking $pIC_{50}$ values across all screened samples for each chemotherapeutic regimen from most sensitive (0%) to most resistant (100%) model to establish a MOS drug response score. We compared MOS sensitivity with the regimen the patient had received to alternative oxaliplatin- (FOLFOX) or irinotecan-based (FOLFIRI/FOLFOXIRI) regimens (Data Supplement, Fig S3A). Most MOS models displayed similar sensitivity to either regimen, whereas others displayed preferential sensitivity to one specific chemotherapy regimen. This suggests that, in a clinical setting, differential responses to these different regimens may be expected.

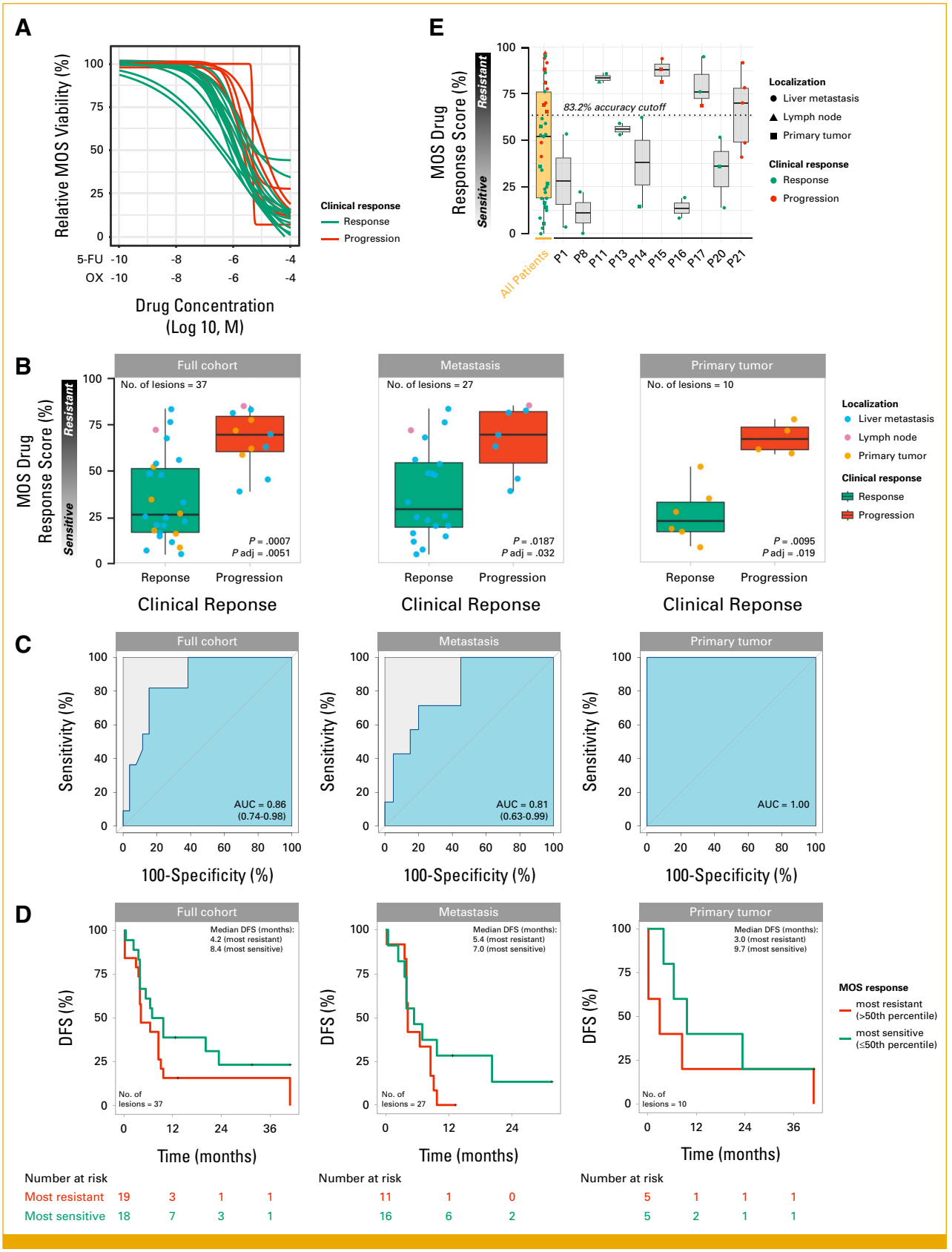


**FIG 3.** In vitro MOS response recapitulates patient response to chemotherapy. (A) Dose-response curves of 19 MOS models exposed to FOLFOX in vitro. Relative viability represents the viability of drug treated conditions normalized to vehicle (=100%) and staurosporine (=0%) controls. Green and red lines represent MOS models derived from lesions that showed clinical response or progression based on TRG (primary) or RECIST-like scoring (metastases). (B) Comparison of MOS drug response score between lesions that showed clinical response or progression in the full cohort (n = 37 lesions from n = 21 patients), metastasis (n = 27 lesions from n = 16 patients), and

**FIG 3.** (Continued). primary tumor (n = 10 lesions from n = 9 patients) groups. Each point indicates a patient-derived MOS model, and the color indicates tumor origin. Blue = liver metastases, pink = lymph node metastasis, and orange = primary tumor. Statistical significance was assessed using the Wilcoxon rank-sum test, and *P* values were adjusted for multiple comparisons using the Benjamini-Hochberg method. (C) ROC curves for predicting treatment response corresponding to the respective box plots in (B). The curves illustrate the trade-off between sensitivity and specificity across a sliding threshold, with the diagonal line representing an $AUC_{ROC}$ of 0.5. AUC is displayed in the plot body, followed by 95% confidence intervals in parentheses. (D) Kaplan-Meier curves depicting the DFS in the full cohort (n = 21 patients), metastasis (n = 16 patients), and primary tumor (n = 9 patients) groups, using a cutoff at the 50th percentile of ranked $pIC_{50}$s. Groups were compared using the Mantel-Cox log-rank test, and *P* values were adjusted for multiple comparisons using the Benjamini-Hochberg method. (E) MOS drug response score for all patients (yellow; n = 37) and for patients from whom ≥2 lesions were sampled (gray, n = 10). Each point represents a patient-derived MOS model, and the shape indicates tumor origin. Color indicates clinical response of the particular lesion as response (green) or progression (red). The dotted line indicates the 83.2% accuracy cutoff defined by the ROC analysis in (C). DFS, disease-free survival; MOS, MicroOrganoSphere; ROC, receiver operating characteristic; TRG, tumor regression grade.



### *Correlation of MOS Response With Clinical Patient Response*

Next, in vitro MOS response was linked to lesion-specific clinical outcomes, with operator blinding ensured by releasing clinical data only postscreening. We integrated gold-standard pathologic evaluation for primary tumors, providing a direct measure of tumor regression, with practical, real-time radiologic response for metastatic settings where TRG is often unavailable (Methods).

MOS-based in vitro response recapitulated lesion-specific clinical response, with statistically significantly greater chemoresistance observed in samples that showed clinical progression in patient-naïve analyses (Wilcoxon $P_{adj}$ = .005, $P_{adj}$ = .032 and $P_{adj}$ = .019 for all, metastatic and primary tumors, respectively; Fig 3B). After accounting for within-cluster correlation with patient-level permutation testing, the association between MOS response and clinical outcome remained significant for all and primary ($P$ = .012 and $P$ = .016), but not for metastatic tumors ($P$ = .212). In addition, we attempted a three-tier classification, distinguishing mild from strong responses and progression (Data Supplement, Fig S3B). Lesion-naïve analysis showed significant differences between the mild and strong response groups from the progression group ($P_{adj}$ = .024 and $P_{adj}$ = .0003, respectively) in the full cohort, which were maintained after patient-level permutation analysis ($P_{adj}$ = .039 and $P_{adj}$ = .001, respectively).

ROC analysis (Fig 3C), using binary classification, revealed that the assay discriminated responders from nonresponders with an AUC of 0.86 (95% CI, 0.74 to 0.98) in the complete cohort (n = 37 lesions from n = 21 patients). At the prespecified cutoff maximizing balanced sensitivity and specificity, the assay showed 83% accuracy (95% CI, 69 to 100), 82% sensitivity (95% CI, 64 to 100), and 85% specificity (95% CI, 64 to 100). For metastases (n = 27 lesions from n = 16 patients), the AUC was 0.81 (95% CI, 0.63 to 0.99), the accuracy was 76% (95% CI, 59 to 78), the sensitivity was 71% (95% CI, 60 to 100), and the specificity was 80% (95% CI, 56 to 100). When predicting clinical response based on primary tumor samples alone (n = 10 lesions from n = 9 patients), assay performed with 100% accuracy (sensitivity = 100%, specificity = 100%, $AUC_{ROC}$ = 1.00).

Using DFS, correlation was assessed at the patient—rather than lesion—level. MOS models were classified as sensitive or resistant using a MOS drug response score cutoff at the 50th percentile. Median DFS was higher in the responder group for all patients combined, patients with sampled metastatic lesions only, and patients with sampled primary lesions only. Separation of the responders and nonresponders was also visible in Kaplan-Meier plots (Fig 3D). Results were not statistically significant with a patient-naïve log-rank test ($P$ = .133, $P$ = .165, $P$ = .282, respectively), nor after a subsequent patient-level permutation analysis ($P$ = .310, $P$ = .388, $P$ = .346, respectively). This indicates that larger patient cohorts will be required to establish statistical significance despite the presence of clear trends in the current study. Taken together, these findings demonstrate that patient-derived MOS models accurately recapitulate clinical response and highlight the potential of using a MOS-based assay for patient stratification.

### *Multilesion Analysis Reveals Intrapatient Heterogeneity*

MOS chemosensitivity data for multiple lesions from different anatomic locations were available for 10 patients, enabling the detection of intrapatient lesion-specific differences in drug response (Fig 3E). For 7 of 10 patients from whom ≥2 samples were collected, prediction of clinical response would have been accurate regardless of which sample (n = 16) was measured in the MOS assay. Patient 11 would be misclassified as a nonresponder, regardless of which of the two included lesions would have been sampled. For the remaining two patients, it depends on which lesion was tested if prediction would have been accurate. Finally, for all patients in this subcohort from whom a primary tumor sample was obtained (n = 4; P14/P15/P17/P20), the primary tumor consistently predicted clinical response accurately. This observation is particularly relevant for potential future clinical applications, where the primary tumor provides the earliest histopathologic confirmation of CRC.

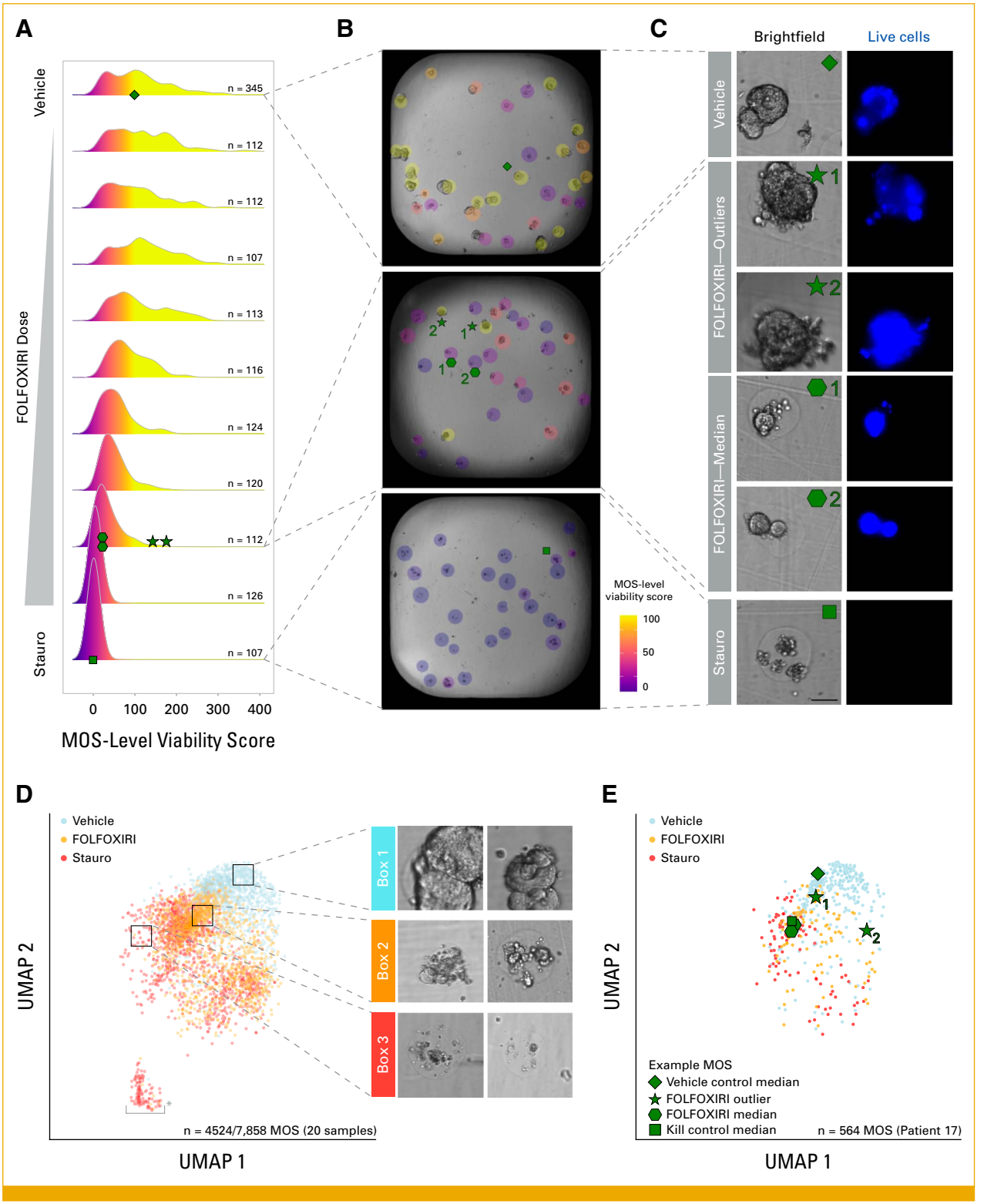


**FIG 4.** Single MOS analysis to detect intratumoral heterogeneity in chemotherapy response. (A) Density plot indicating the distribution of EpCAM-based relative viability per individual MOS in FOLFOXIRI-treated and control conditions for a single donor sample (P17/S26). Green symbols indicate individual MOS highlighted in panels (B, C, and E). Diamond indicates one individual MOS at the median of the vehicle control condition, hexagons indicate individual MOS at the median of high-dose (68.6 nM SN-38) FOLFOXIRI, stars indicate outlier MOS in high-dose FOLFOXIRI, and square indicates one individual MOS at the median of the staurosporine control. Color scale indicates the MOS-level viability score, defined as EpCAM-based relative viability per individual MOS (Methods). N indicates the number of MOS in each condition. (B) Well-level brightfield images of vehicle (top), high-dose (68.6 nM SN-38) FOLFOXIRI (middle), and staurosporine (bottom) conditions. Transparent overlays indicate individual MOS and are colored by MOS-level viability score. Green symbols indicate matching MOS to panels (A), (C), and (E) as described above. (C) Enlarged (continued on following page)

**FIG 4.** (Continued). brightfield (left) and Calcein AM (right) images depicting MOS of interest. Green symbols indicate example MOS shown in panels (A, B, and E). Scale bar = 100 μm. (D) Left panel: Unsupervised 2D representation of MOS brightfield images via UMAP projections of DINOv2 embeddings. Equal numbers of images are plotted from each of three categories across all samples in the cohort that were assayed with FOLFOXIRI (20 total). Colored points indicate sampled MOS from the following conditions: vehicle (blue), high-dose FOLFOXIRI (68.7 nM SN-38, orange), and staurosporine (red); bracket in lower left indicates the cluster of empty images resulting from rare technical artifacts (1.1% for the full data set under described conditions). Right panel: Representative brightfield images of MOS whose UMAP projections are located in boxes in (D). Box 1: UMAP area enriched for vehicle control; Box 2: UMAP area enriched for high-dose (68.7 nM SN-38) FOLFOXIRI; Box 3: UMAP area enriched for staurosporine control. Filters identical to those used in the MOS-level heterogeneity analysis (Methods) were applied to remove MOS with characteristics that may confound drug treatment comparisons before visualization, for the analyses depicted here and in panel (E). (E) Unsupervised 2D representation of MOS brightfield images via UMAP projections of DinoV2 encodings paralleling MOS outlier vignette for one MOS model (P17/S26). Colored points indicate MOS from different conditions: vehicle (blue), high-dose (68.7 nM SN-38) FOLFOXIRI (orange), and staurosporine (red). Green symbols indicate matching MOS to (A-C). FOLFOXIRI, infusional fluorouracil, leucovorin, oxaliplatin, and irinotecan; MOS, MicroOrganoSphere; UMAP, Uniform Manifold Approximation and Projection.



### Single MOS Analysis Enables Detection of Intratumoral Heterogeneity in Chemotherapy Response

#### *Intratumoral Heterogeneity Quantification Using Single MOS Analysis and Identification of Drug-Resistant Clones*

To explore if MOS can be used to measure heterogeneity in drug response within one sample, we used images segmented at the MOS level to calculate single MOS relative viability (Methods). We normalized this viability against vehicle controls dimethyl sulfoxide (DMSO) and staurosporine-treated kill controls (Fig 4A, showing results for P17/S26). As expected, the median viability signal of individual MOS decreased with increasing chemotherapy concentrations. Interestingly, a wide distribution of MOS viability within each treated well was observed, indicating that PDTOs derived from the same tumor sample maintain heterogeneous drug responses, a finding in line with previous studies.[30-32] Projection of single MOS-level viability scores onto brightfield images visually confirmed this heterogeneous tumor cell outgrowth in MOS derived from single samples (Fig 4B, Data Supplement, Fig S4A).

At high chemotherapy doses, some of the tested samples showed outlier MOS that exhibited high viability at the assay end point, suggesting that tumor cells within these MOS continue to proliferate despite the presence of chemotherapy concentrations toxic to most neighboring tumor cells. Inspection of brightfield images of these seemingly drug-resistant MOS (defined as MOS-level viability score >5× median for the drug treatment condition) provides visual confirmation that they contain higher biomass than most of their counterparts (median ±5%; Fig 4C, Data Supplement, Fig S4B). This observation illustrates the MOS platform's potential to capture and model intratumoral heterogeneity of drug response in vitro.

#### *MOS Phenotyping via Brightfield Imaging*

Machine learning models trained on brightfield imaging can predict cellular and disease phenotypes and are increasingly used in drug development.[33] Here, we asked if brightfield imaging can capture drug response MOS phenotypes. DINOv2[34] embeddings of individual MOS images were visualized using the Uniform Manifold Approximation and Projection (UMAP) algorithm, revealing treatment-specific (vehicle controls, kill controls, and FOLFOXIRI) clustering of end point MOS images (Fig 4D). Cropped single-MOS images from different regions of the UMAP confirmed expected morphological characteristics of highly proliferative (Fig 4D, box 1), partially arrested (Fig 4D, box 2), and growth-arrested (Fig 4D, box 3) MOS. Based on brightfield imaging only, FOLFOXIRI-resistant outlier MOS that were previously identified by EpCAM-based measurement (Methods, Figs 4A-4C) clustered closer to DMSO-treated than to median FOLFOXIRI- or staurosporine-treated MOS (Fig 4E; mean UMAP distance from FOLFOXIRI outliers: DMSO = 2.08; FOLFOXIRI median = 2.71; Stauro = 3.68). In addition to biological phenotypes, technical factors such as MOS position, movement, air bubbles, or plate mishandling were also captured (Data Supplement, Fig S5). These results suggest that supervised models may ultimately enable brightfield-only readout of MOS drug response providing a low-cost, scalable, live imaging assay.

## DISCUSSION

We previously presented proof-of-concept data indicating that MOS-based ex vivo screening recapitulates clinical response to chemotherapy.[21,22] Here, we have applied MOS-based functional precision medicine to a larger retrospective cohort of patients with CRC to validate its potential to inform clinical decision making.

In vitro MOS drug testing recapitulated lesion-specific clinical response to standard-of-care chemotherapies with 83% accuracy (82% specificity, 85% sensitivity), exceeding the pooled accuracy reported for classical CRC PDTOs (76%; 79% sensitivity, 75% specificity).[17] This superior performance may reflect the assay's demonstrated reproducibility and standardization. For primary tumors, the assay showed 100% sensitivity and 100% specificity, although in a limited cohort (n = 10). This difference might reflect the higher clonal complexity of primary tumors, containing more sensitive clones, or the greater burden of previous treatment of metastases.

Resistance to standard-of-care regimens is a major clinical challenge in advanced CRC.[35] Extensive preclinical work tries to identify resistance mechanisms to chemotherapy or targeted therapies.[35,36] By enabling high-throughput, live imaging of resistant MOS, our approach provides a scalable method to study intratumoral heterogeneity and dissect fundamental mechanisms of resistance. In addition, resistance scoring might yield additional precision for patient outcomes in future investigations.

Together, these findings support the clinical potential of the MOS platform as a decision-making tool that could increase response rates by individualizing the patient journey.

Despite encouraging results, limitations of this study include the cohort's modest size and heterogeneous clinical characteristics, which may limit the generalizability of the current study. Prospective studies in larger cohorts are needed to validate the predictive potential of MOS-based screening. Despite technical advances in standardization and automation, regulatory and reimbursement hurdles remain barriers for adoption in clinical practice.

In addition, future studies will focus on establishing MOS directly from primary dissociated tumor cells, further reducing the turnaround time in a diagnostic setting. Moreover, MOS generated directly from tumor tissue retain the nontumor components of the tumor microenvironment (TME)[21] and further reduce the risk of genetic drift and selection. This will enable assessment of TME-engaging therapies to kill tumor cells such as immune checkpoint inhibitors or TME-targeting antibodies.



## AFFILIATIONS

[1]Xilis B.V., Utrecht, the Netherlands
[2]Cancer Progression and Metastasis Group, German Cancer Research Center (DKFZ) and DKFZ-ZMBH Alliance, Heidelberg, Germany
[3]Department of General, Visceral and Transplant Surgery, University Hospital Heidelberg, Heidelberg, Germany
[4]Xilis Inc, Durham, NC
[5]Heidelberg Institute for Stem Cell Technology and Experimental Medicine (HI-STEM gGmbH), Heidelberg, Germany
[6]Faculty of Biosciences, Heidelberg University, Heidelberg, Germany
[7]Junior Research Group Epithelium Microbiome Interactions (EMIL), German Cancer Research Center, Heidelberg, Germany
[8]DKFZ Hector Cancer Institute at the University Medical Center, Mannheim, Germany
[9]NCT Heidelberg, A Partnership Between DKFZ and University Medical Center Heidelberg, Heidelberg, Germany
[10]Department of Applied Tumor Biology, Institute of Pathology, Heidelberg University Hospital, Heidelberg, Germany
[11]Department of Medical Oncology, National Center for Tumor Diseases (NCT) Heidelberg, Heidelberg University Hospital, Heidelberg, Germany
[12]Department of Hematology and Oncology, University Hospital of Schleswig-Holstein, Lübeck, Germany
[13]German Cancer Consortium (DKTK), German Cancer Research Center (DKFZ), Heidelberg, Germany

## CORRESPONDING AUTHOR

Else Driehuis, PhD; e-mail: else.driehuis@xilis.nl.

## EQUAL CONTRIBUTION

R.G. and N.S. contributed equally to this work. B.K., E.D., and R.J. share last authorship.

## PRIOR PRESENTATION

Presented in part at ASCO Annual Meeting, Chicago, IL, May 30-June 3, 2025; and at ESMO Congress, Berlin, Germany, October 17-21, 2025.

## SUPPORT

Supported by Oncode Accelerator, a Dutch National Growth Fund project (NGFOP220), Dietmar Hopp Foundation, and by the Dr Rolf M. Schwiete Foundation, the Deutsche Forschungsgemeinschaft DFG (JA 2558/3-1; JA 2558/4-1; JA 2558/6-1; JA 2558/9-1 P06 [FOR 5806]), and BMBF-funded SATURN3 project (01KD2206B; 01KD2206E) to R.J; and by the Clinician Scientist Program of the Medical Faculty, Heidelberg University to N.S.

## DATA SHARING STATEMENT

A data sharing statement provided by the authors is available with this article at DOI https://doi.org/10.1200/PO-25-00501.

## AUTHOR CONTRIBUTIONS

**Conception and design:** Roán Gobits, Nikolai Schleußner, Sylvia W.F. Suen, Eric Daniel Bankaitis, Kevin Brown, Daniel A. Nelson, Corey Evans, Thomas Schmidt, Dennis Plenker, Ryan T. Jones, Bruno Köhler, Else Driehuis, Rene Jackstadt
**Administrative support:** Eric Struminger, Corey Evans, Thomas Schmidt, Carlton Barnett, Ryan T. Jones
**Provision of study materials or patients:** Nikolai Schleußner, Martin Schneider, Thomas Schmidt
**Collection and assembly of data:** Roán Gobits, Nikolai Schleußner, Gavin R. Oliver, Sylvia W.F. Suen, Mandy P.M. Koomen, Francesca Paolucci, Kilian Martens, Aitana Guiseris Martinez, Julia Volk, Carolin Artmann, Manuel Mastel, Matthias Kloor, Eric Daniel Bankaitis, Hayden Eric Stoub, Jens Puschhof, Kevin Brown, Sebastian Pretzer, Daniel A. Nelson, Eric Struminger, Amelia Zessin, Amanda Brown, Daniel Yetsko, Mackenzie Harrington, Gabriel Salg, Martin Schneider, Thomas Schmidt, Dennis Plenker, Bruno Köhler, Else Driehuis, Rene Jackstadt
**Data analysis and interpretation:** Roán Gobits, Gavin R. Oliver, Michael Rutenberg Schoenberg, António Miguel de Jesus Domingues, Pavan Ramkumar, Aitana Guiseris Martinez, Kyanna S. Ouyang, Eric Daniel Bankaitis, Hayden Eric Stoub, Jens Puschhof, Kevin Brown, Daniel A. Nelson, Thomas Schmidt, Elena Helman, Dennis Plenker, Carlton Barnett, Bruno Köhler, Else Driehuis, Rene Jackstadt
**Manuscript writing:** All authors
**Final approval of manuscript:** All authors
**Accountable for all aspects of the work:** All authors

## AUTHORS' DISCLOSURES OF POTENTIAL CONFLICTS OF INTEREST

The following represents disclosure information provided by authors of this manuscript. All relationships are considered compensated unless otherwise noted. Relationships are self-held unless noted. I = Immediate Family Member, Inst = My Institution. Relationships may not relate to the subject matter of this manuscript. For more information

about ASCO's conflict of interest policy, please refer to www.asco.org/rwc or ascopubs.org/po/author-center.
Open Payments is a public database containing information reported by companies about payments made to US-licensed physicians (Open Payments).

**Roán Gobits**
**Employment:** Xilis B.V

**Michael Rutenberg Schoenberg**
**Employment:** Xilis, Arrakis Therapeutics
**Stock and Other Ownership Interests:** Xilis

**António Miguel de Jesus Domingues**
**Employment:** Xilis B.V

**Pavan Ramkumar**
**Employment:** Xilis
**Consulting or Advisory Role:** Xilis, Verge Genomics
**Travel, Accommodations, Expenses:** Xilis

**Hayden Eric Stoub**
**Employment:** Xilis
**Consulting or Advisory Role:** IORGANBIO
**Travel, Accommodations, Expenses:** IORGANBIO

**Jens Puschhof**
**Consulting or Advisory Role:** Nanokur, Allergopharma
**Research Funding:** Emulate (Inst)
**Patents, Royalties, Other Intellectual Property:** J.P. discloses patents related to organoid technology

**Kevin Brown**
**Employment:** Xilis, Intuitive Surgical
**Stock and Other Ownership Interests:** Intuitive Surgical
**Travel, Accommodations, Expenses:** Intuitive Surgical

**Eric Struminger**
**Employment:** Xilis, Steps for Recovery (I)
**Leadership:** Xilis
**Stock and Other Ownership Interests:** Xilis

**Amelia Zessin**
**Employment:** Xilis

**Corey Evans**
**Employment:** Xilis

**Daniel Yetsko**
**Employment:** Xilis
**Stock and Other Ownership Interests:** Xilis
**Research Funding:** Xilis

**Elena Helman**
**Employment:** Xilis, Ultima Genomics
**Leadership:** Xilis, Ultima Genomics
**Stock and Other Ownership Interests:** Ultima Genomics
**Patents, Royalties, Other Intellectual Property:** I hold patents for algorithms related to Tumor Mutational Burden, Homologous Recombination, ctDNA dynamics
**Travel, Accommodations, Expenses:** Xilis

**Dennis Plenker**
**Stock and Other Ownership Interests:** Xilis

**Carlton Barnett**
**Employment:** Xilis
**Leadership:** 7 Hills Pharma
**Stock and Other Ownership Interests:** Xilis

**Ryan T. Jones**
**Employment:** Xilis

**Bruno Köhler**
**Consulting or Advisory Role:** SERVIER, Pierre Fabre
**Speakers' Bureau:** BMS GmbH & Co. KG, Takeda
**Research Funding:** AbbVie, Gilead Sciences
**Travel, Accommodations, Expenses:** Pierre Fabre

**Else Driehuis**
**Employment:** Xilis BV
**Patents, Royalties, Other Intellectual Property:** Listed as inventor on patent related to head & neck organoid models

No other potential conflicts of interest were reported.

## ACKNOWLEDGMENT

We thank all patients participating in this study and the teams approaching patients for consent and collecting tissue. Additionally, we thank Lennart Kester and Erik Bus, from the Diagnostics department of the Princess Máxima Center, for developing, validating, and sharing the gene panel used for SNP fingerprinting. We thank the histology team and Domenico Castigliego of the Pathology department of the UMCU for performing immunohistochemical stainings of the PDTOs and tumor tissue. We also thank Matthias Kloor of the Department of Applied Tumor Biology, Institute of Pathology, Heidelberg University Hospital, Heidelberg, Germany, for performing immunohistochemical stainings to confirm MMR status.

## REFERENCES

1. Bray F, Laversanne M, Sung H, et al: Global cancer statistics 2022: GLOBOCAN estimates of incidence and mortality worldwide for 36 cancers in 185 countries. CA Cancer J Clin 74:229-263, 2024
2. Xi Y, Xu P: Global colorectal cancer burden in 2020 and projections to 2040. Transl Oncol 14:101174, 2021
3. Siegel RL, Wagle NS, Cercek A, et al: Colorectal cancer statistics, 2023. CA Cancer J Clin 73:233-254, 2023
4. Hossain MS, Karuniawati H, Jairoun AA, et al: Colorectal cancer: A review of carcinogenesis, global epidemiology, current challenges, risk factors, preventive and treatment strategies. Cancers 14: 1732, 2022
5. Morton D, Seymour M, Magill L, et al: Preoperative chemotherapy for operable colon cancer: Mature results of an international randomized controlled trial. J Clin Oncol 41:1541-1552, 2023
6. Nordlinger B, Sorbye H, Glimelius B, et al: Perioperative FOLFOX4 chemotherapy and surgery versus surgery alone for resectable liver metastases from colorectal cancer (EORTC 40983): Long-term results of a randomised, controlled, phase 3 trial. Lancet Oncol 14:1208-1215, 2013
7. Kanemitsu Y, Shimizu Y, Mizusawa J, et al: Hepatectomy followed by mFOLFOX6 versus hepatectomy alone for liver-only metastatic colorectal cancer (JCOG0603): A phase II or III randomized controlled trial. J Clin Oncol 39:3789-3799, 2021
8. Gustavsson B, Carlsson G, Machover D, et al: A review of the evolution of systemic chemotherapy in the management of colorectal cancer. Clin Colorectal Cancer 14:1-10, 2015
9. Kawai S, Takeshima N, Hayasaka Y, et al: Comparison of irinotecan and oxaliplatin as the first-line therapies for metastatic colorectal cancer: A meta-analysis. BMC Cancer 21:116, 2021
10. Koopman, M, Venderbosch, S, Nagtegaal, ID, et al: A review on the use of molecular markers of cytotoxic therapy for colorectal cancer, what have we learned? Eur J Cancer 45:1935-1949, 2009.
11. Garnett MJ, Edelman EJ, Heidorn SJ, et al: Systematic identification of genomic markers of drug sensitivity in cancer cells. Nature 483:570-575, 2012
12. Punt CJA, Koopman M, Vermeulen L: From tumour heterogeneity to advances in precision treatment of colorectal cancer. Nat Rev Clin Oncol 14:235-246, 2017
13. Koncina E, Haan S, Rauh S, et al: Prognostic and predictive molecular biomarkers for colorectal cancer: Updates and challenges. Cancers 12:319, 2020
14. Drost J, Clevers H: Organoids in cancer research. Nat Rev Cancer 18:407-418, 2018
15. Wensink GE, Elias SG, Mullenders J, et al: Patient-derived organoids as a predictive biomarker for treatment response in cancer patients. NPJ Precis Oncol 5:30, 2021
16. Vlachogiannis G, Hedayat S, Vatsiou A, et al: Patient-derived organoids model treatment response of metastatic gastrointestinal cancers. Science 359:920-926, 2018

17. Sakshaug BC, Folkesson E, Haukaas TH, et al: Systematic review: Predictive value of organoids in colorectal cancer. Sci Rep 13:18124, 2023
18. Smabers LP, Wensink E, Verissimo CS, et al: Organoids as a biomarker for personalized treatment in metastatic colorectal cancer: Drug screen optimization and correlation with patient response. J Exp Clin Cancer Res 43:61, 2024
19. Veninga V, Voest EE: Tumor organoids: Opportunities and challenges to guide precision medicine. Cancer Cell 39:1190-1201, 2021
20. van der Graaff D, Seghers S, Vanclooster P, et al: Advancements in research and treatment applications of patient-derived tumor organoids in colorectal cancer. Cancers 16:2671, 2024
21. Ding S, Hsu C, Wang Z, et al: Patient-derived micro-organospheres enable clinical precision oncology. Cell Stem Cell 29:905-917.e6, 2022
22. Wang Z, Boretto M, Millen R, et al: Rapid tissue prototyping with micro-organospheres. Stem Cel Rep 17:1959-1975, 2022
23. Eisenhauer, EA, Therasse, P, Bogaerts, J, et al: New response evaluation criteria in solid tumours: Revised RECIST guideline (version 1.1). Eur J Cancer 45:228-247, 2009
24. Dworak O, Keilholz L, Hoffmann A: Pathological features of rectal cancer after preoperative radiochemotherapy. Int J Colorectal Dis 12:19-23, 1997
25. Bolboacă SD: Medical diagnostic tests: A review of test anatomy, phases, and statistical treatment of data. Comput Math Methods Med 2019:1891569, 2019
26. Selliah N, Eck S, Green C, et al: Flow cytometry method validation protocols. Curr Protoc Cytom 87:e53, 2019
27. Fujii M, Matano M, Toshimitsu K, et al: Human intestinal organoids maintain self-renewal capacity and cellular diversity in niche-inspired culture condition. Cell Stem Cell 23:787-793.e6, 2018
28. Armaghany T, Wilson JD, Chu Q, et al: Genetic alterations in colorectal cancer. Gastrointest Cancer Res 5:19-27, 2012
29. Yaeger R, Chatila WK, Lipsyc MD, et al: Clinical sequencing defines the genomic landscape of metastatic colorectal cancer. Cancer Cell 33:125-136.e3, 2018
30. Coppo R, Kondo J, Iida K, et al: Distinct but interchangeable subpopulations of colorectal cancer cells with different growth fates and drug sensitivity. iScience 26:105962, 2023
31. Roerink SF, Sasaki N, Lee-Six H, et al: Intra-tumour diversification in colorectal cancer at the single-cell level. Nature 556:457-462, 2018
32. Sharick JT, Walsh CM, Sprackling CM, et al: Metabolic heterogeneity in patient tumor-derived organoids by primary site and drug treatment. Front Oncol 10:553, 2020
33. Harrison PJ, Gupta A, Rietdijk J, et al: Evaluating the utility of brightfield image data for mechanism of action prediction. PLoS Comput Biol 19:e1011323, 2023
34. Oquab M, Darcet T, Moutakanni T, et al: DINOv2: Learning robust visual features without supervision. 2024. https://doi.org/10.48550/arXiv.2304.07193
35. Boumahdi S, de Sauvage FJ: The great escape: Tumour cell plasticity in resistance to targeted therapy. Nat Rev Drug Discov 19:39-56, 2020
36. Russo M, Chen M, Mariella E, et al: Cancer drug-tolerant persister cells: From biological questions to clinical opportunities. Nat Rev Cancer 24:694-717, 2024